Crack detection in prestressed concrete structures by measuring their natural frequencies

G. D. Ercolani, D. H. Felix & N. F. Ortega

Springer

Springer

ORIGINAL PAPER

CrossMark

Crack detection in prestressed concrete structures by measuring their natural frequencies

G. D. Ercolani[1,2] · D. H. Felix[1] · N. F. Ortega[1,3]

Abstract

When inspecting the health of a civil structure, it is important to have efficient techniques to detect the possible presence of structural damage. This work deals with the detection of damage in prestressed concrete structures, which are widely used in road bridges and long span slabs, among others. Concrete structures can be affected by different pathologies, with the transverse cracks beingone of the most dangerous damages, since they involve a localized reduction of the flexural rigidity of the structure. Such cracks change both the static and dynamic behavior of the structure. In this paper, an inverse method of damage detection is applied on two experimental beams built in the laboratory, from the measurement of the first three natural frequencies of vibration. An algorithm for solving the system of equations has been developed by the authors. Explicit equations were obtained to calculate both the crack position and its depth. The predicted damages by the algorithm have been in good agreement with the real damages of the experimental models. An important aspect of this methodology for crack detection is the simplicity of its experimental implementation.

Keywords Prestressed concrete · Crack detection · Natural frequencies · Inverse method · Dynamic tests

1 Introduction

Prestressed concrete structures often suffer various kinds of damage throughout their service life; therefore, it is extremely important to identify them, as soon as possible, to take effective preventive actions for the health of the structure. Several pathologies can affect the prestressed concrete structures; many of them are manifested by the appearance of cracks. As a consequence, numerous studies about cracks in prestressed concrete have emerged in recent times [1–3].

In many cases, depending on the extent of the damage and its velocity of propagation, a cracked concrete structure can work correctly from the point of view of its structural function. Nevertheless, such damage deserves attention because it can mean a potential risk to the safety of the structure. It must also be taken into account that the presence of cracks in the concrete can promote the corrosion of steel. In addition, corrosion occurs more rapidly under high tensile stress, which is why it is especially important in prestressed concrete structures [4, 5].

Among the pathologies which can affect a prestressed concrete structure, the present approach deals with damage manifested through typical bending cracks. These cracks are normal to the axis of the beam and deeper in correspondence with the higher tensile stresses. The width of the bending cracks is variable, being wider at the bottom and closing toward the top. Several causes can promote bending cracks in prestressed concrete beams, namely the decrease of the prestressing force that takes place with time, excessive loads, constructive defects and differential settlements in hyperstatic structures, among others [6].

Regarding the influence of the maximum crack width in the corrosion process, several standards, especially those based on the CEB-FIP Model Code [7], determine a "Cracking Limit State" by which the mechanical strength and durability of the structure should not be affected. As an

✉ G. D. Ercolani
german.ercolani@uns.edu.ar

1 Instituto de Ingeniería, Departamento de Ingeniería, Universidad Nacional del Sur, Bahía Blanca, Argentina

2 Consejo Nacional de Investigaciones Científicas y Técnicas, Buenos Aires, Argentina

3 Comisión de Investigaciones Científicas de la Prov. de Buenos Aires, Buenos Aires, Argentina

example, the standard EHE-08 [8] determines the maximum crack width for structural concrete elements in the absence of special requirements (e.g., sealing) and for different exposure environments, regardless of the causes of the cracks. In the case of prestressed concrete, the standard determines a maximum crack width of 0.20 mm for non-aggressive or normal environments, while it does not admit cracks for marine or chemically aggressive environments. On the other hand, CIRSOC 201 [9], inspired by ACI 318 [10], establishes limitations for the separation of reinforcements to control the cracking caused by the bending stresses; however, this standard does not impose a maximum allowable crack width.

A particularity in prestressed concrete structures, with respect to reinforced concrete, is that the prestressing action tends to keep the cracks closed after the causes of cracking have disappeared. This can make the detection of damages difficult in prestressed concrete structures for early damage states [11]. For this reason, it is necessary to validate and adjust a method specified as inverse method (IM), frequently used to control the health of reinforced concrete structures. This crack detection method is based on the dynamic response of the structure and, in this work, has been applied to experimental models of prestressed concrete beams.

The presence of a crack in a beam affects in different ways its natural frequencies of vibration according to the magnitude and the location of the crack. This is the basis of the IM for the detection of damage in the structure. The most simple and accepted way to represent the decrease of stiffness, at the crack location, is by using a rotational spring. In addition, the stiffness of the rotational spring can be related to the depth of the crack, by means of the fracture mechanics theory [12, 13].

Rizos et al. [14] demonstrated the use of the model of rotational spring along with the modal analysis technique for identification of crack location and magnitude in a cantilever beam. Liang et al. [15] demonstrated the validity of the inverse method in a uniform beam under simply supported or cantilever boundary conditions. Nandwana and Maiti [16] have applied this method to models of beams in the presence of an inclined edge, or internal normal cracks. Rosales et al. [17] present two approaches: the solution of the inverse problem with a power series technique (PST) and the use of artificial neural networks (ANNs) in a cantilever beam. Orbanich et al. [18] use this method for the detection of cracks, in numerical and experimental models of reinforced concrete. Mazanoglu and Sabuncu [19] deal with numerical and experimental models of cantilever beams of steel, with one single crack and double cracks. Barad et al. [20] also obtain good results in experimental models of cantilever beams with a crack.

However, no applications of the inverse method have been found in prestressed concrete structures.

2 Fundamentals of the inverse method

In this work, the IM is applied to find the location and magnitude of a discrete crack present in a beam from the measurement of its first three natural frequencies of vibration. To understand the fundamentals of the IM, the direct problem for homogeneous linear elastic material and constant cross section is first presented. This means that the first three natural frequencies are obtained for a model with damage previously defined and it is analyzed how they are modified depending on the location and depth of the crack.

In the model shown in Fig. 1, the crack is represented by a rotational spring with a stiffness k_r, located at the position αL measured from the left end of the beam, where L is the total length of the beam. The rotational spring introduces a singularity that divides the beam into two parts. Then the mode shape for each part is obtained [21]:

$$v_1(x) = A_1\cos(\beta x) + A_2\text{sen}(\beta x) + A_3\cosh(\beta x) + A_4\text{senh}(\beta x), \tag{1}$$

$$v_2(x) = B_1\cos(\beta x) + B_2\text{sen}(\beta x) + B_3\cosh(\beta x) + B_4\text{senh}(\beta x), \tag{2}$$

where v_1 and v_2 are the displacements in the y-direction, to the left and right of the crack, respectively; A_i and B_i, with $i = 1, 2, 3, 4$, are constants to be determined from the boundary and continuity conditions; β is the eigenvalue corresponding to the natural frequencies of vibration:

$$\beta = \sqrt{\frac{\varpi}{c}}, \tag{3}$$

in which ω is the natural frequency in *rad/s* and c is a parameter associated with the geometrical and mechanical properties of the beam:

$$c = \sqrt{\frac{EI}{\rho A L^4}}, \tag{4}$$

where E is the elastic modulus of the material; A and I are the area and the moment of inertia for the cross section of the beam, respectively; ρ is the material density; and L is the total length of the beam.

It is noteworthy that for a simply supported beam without damage, the eigenvalues corresponding to the first three natural frequencies are $\beta_1 = \pi$, $\beta_2 = 2\pi$, $\beta_3 = 3\pi$ [22]. In case of a damaged beam, these eigenvalues will be lower due to the loss of structural rigidity. Furthermore, the spring stiffness can also be expressed in a dimensionless way as:
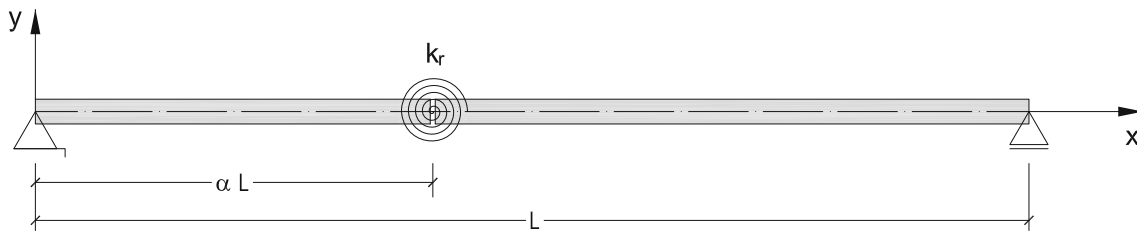
Fig. 1 Simply supported beam with a discrete crack modeled as a rotational spring

$$k = \frac{k_r}{EI/L}. \tag{5}$$

Then the boundary conditions of the beam and the continuity conditions must be applied at the position of the spring. In the case of the simply supported beam represented in Fig. 1, the boundary conditions are associated with zero vertical displacement and zero bending moment in both supports. Taking into account the dimensionless mode, this is:

$$v_1(0) = 0 \quad v_1''(0) = 0 \quad v_2(1) = 0 \quad v_2''(1) = 0, \tag{6}$$

where the conditions of continuity, at the position of the rotational spring, are expressed as follows:

$$\begin{aligned} v_1(\alpha) &= v_2(\alpha) \quad v_1''(\alpha) = v_2''(\alpha) \quad v_1'''(\alpha) = v_2'''(\alpha) \\ v_1''(\alpha) &= k(v_2'(\alpha) \quad - v_1'(\alpha)). \end{aligned} \tag{7}$$

Combining Eqs. (6) and (7) with Eq. (1) and (2), the following matrix is obtained:

following equation obtained from the fracture mechanics theory [12, 13]:

$$k_r = \frac{Ebh^2}{72\pi f(r)}, \tag{9}$$

in which:

$$\begin{aligned} f(r) = {}&0.6384\ r^2 - 1.035\ r^3 + 3.7201\ r^4 + 7.553\ r^6 \\ &+ 7.3324\ r^7 + 2.4909\ r^8. \end{aligned} \tag{10}$$

Then, Eq. (9) can be expressed in the dimensionless mode as follows:

$$k = \frac{\lambda}{6\pi f(r)}, \tag{11}$$

where λ is the slenderness of the beam:

$$\lambda = \frac{L}{h}. \tag{12}$$

$$\begin{bmatrix} 1 & -1 & 0 & 0 & \cos(\alpha\beta) & -\cos(\alpha\beta) & \sin(\alpha\beta) & -\beta\cos(\alpha\beta) - k\sin(\alpha\beta) \\ 0 & 0 & 0 & 0 & \sin(\alpha\beta) & -\sin(\alpha\beta) & -\cos(\alpha\beta) & k\cos(\alpha\beta) - \beta\sin(\alpha\beta) \\ 1 & 1 & 0 & 0 & \cosh(\alpha\beta) & \cosh(\alpha\beta) & \sinh(\alpha\beta) & \beta\cosh(\alpha\beta) + k\sinh(\alpha\beta) \\ 0 & 0 & 0 & 0 & \sinh(\alpha\beta) & \sinh(\alpha\beta) & \cosh(\alpha\beta) & k\cosh(\alpha\beta) + \beta\sinh(\alpha\beta) \\ 0 & 0 & \cos(\beta) & -\cos(\beta) & -\cos(\alpha\beta) & \cos(\alpha\beta) & -\sin(\alpha\beta) & k\sin(\alpha\beta) \\ 0 & 0 & \sin(\beta) & -\sin(\beta) & -\sin(\alpha\beta) & \sin(\alpha\beta) & \cos(\alpha\beta) & -k\cos(\alpha\beta) \\ 0 & 0 & \cosh(\beta) & \cosh(\beta) & -\cosh(\alpha\beta) & -\cosh(\alpha\beta) & -\sinh(\alpha\beta) & -k\sinh(\alpha\beta) \\ 0 & 0 & \sinh(\beta) & \sinh(\beta) & -\sinh(\alpha\beta) & -\sinh(\alpha\beta) & -\cosh(\alpha\beta) & -k\cosh(\alpha\beta) \end{bmatrix}. \tag{8}$$

In matrix (8), the first four columns correspond to each of the four boundary conditions, while the last four columns correspond to each of the four continuity conditions at the position of the spring. Thus, to obtain a non-trivial solution of the system, the determinant of its coefficients must be zero. This gives a relationship between k, α and the eigenvalues β.

Moreover, for a beam of rectangular cross section, of width b and height h, the spring stiffness can be related to the depth parameter r of the crack (Fig. 2), using the

Combining Eq. (11) with the previous development, a direct relationship between r, α and β is obtained. In Figs. 3, 4 and 5, the parametric plots β vs. α have been made for the non-dimensional parameter r in the range between $r = 0$ (without damage) and $r = 0.5$ (when the crack achieves half of the beam height). These plots have been obtained for the slenderness $\lambda = 20$. As expected, it can be noted that when the depth of the crack increases, the beam rigidity decreases and, therefore, the frequency coefficients are reduced. This effect is stronger when the
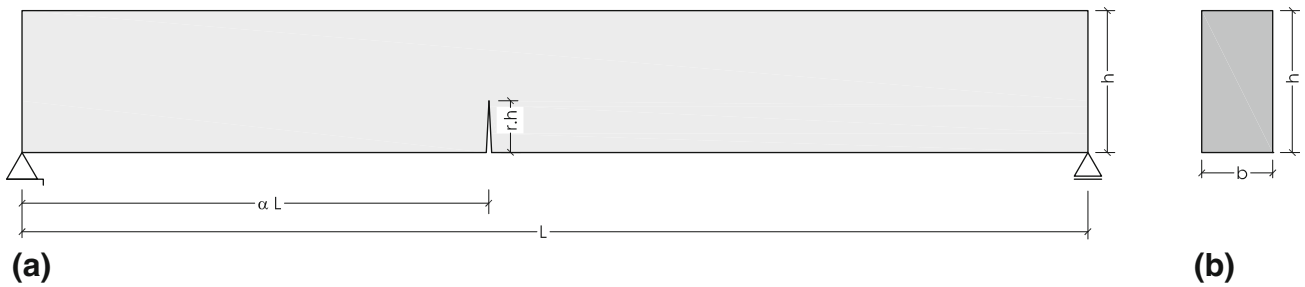
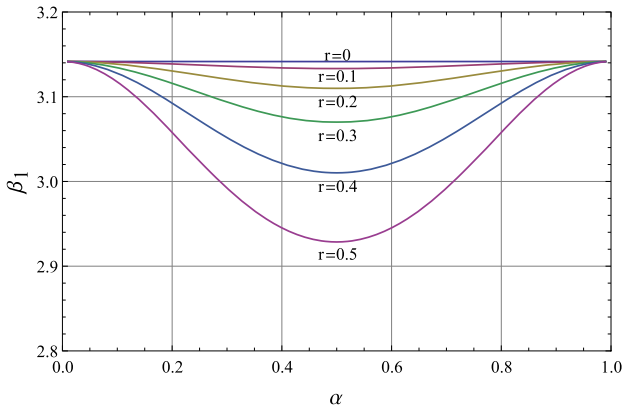**Fig. 2** **a** Longitudinal view of the beam. **b** Cross section of the beam

Fig. 3 Plot of β_1 vs. α, for different values of r, in a simply supported beam with $\lambda = 20$

Fig. 5 Plot of β_3 vs. α, for different values of r, in a simply supported beam with $\lambda = 20$
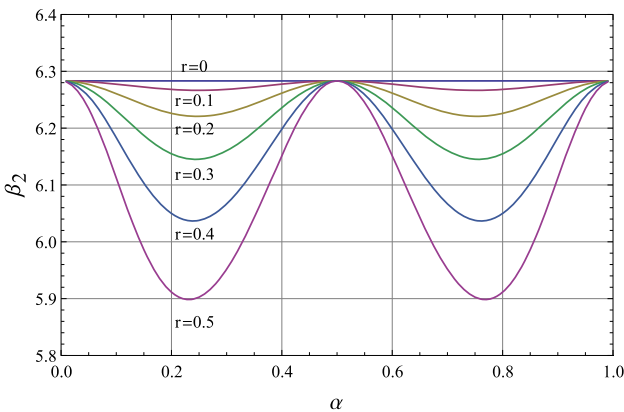
Fig. 4 Plot of β_2 vs. α, for different values of r, in a simply supported beam with $\lambda = 20$

crack is closer to one of the anti-nodes of the modal shape. Instead, when the crack is in the position of one of the nodes, no change is perceived for the natural frequency of vibration.

In the direct problem, k (or r) and α are known and the eigenvalues β are obtained. Instead, in the inverse problem, the eigenvalues β are known and for each of them the stiffness k can be plotted as a function of α. If these curves are plotted for the first three natural frequencies, they will
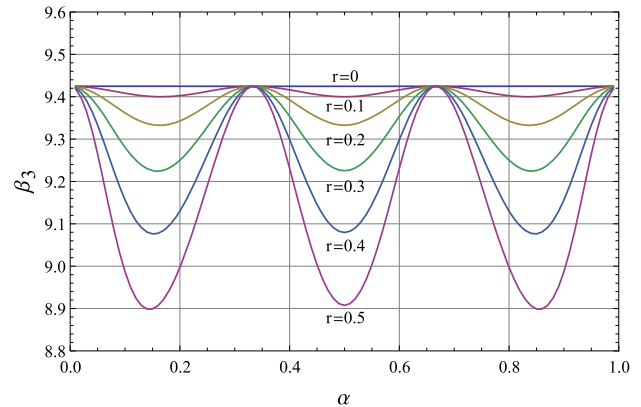
all cross through the point corresponding to k and α of the crack, forming an intersection point. Then this intersection point of the curves k vs. α determines the solution of the inverse problem, giving the position of the crack (α) and the stiffness of the spring (k).

It is worth mentioning that the vibration modes are related to bending modes and it is enough and necessary to use the first three natural frequencies for the purpose of identifying this damage [15]. This is because the first two curves k vs. α intersect each other even when there is no damage in the structure, while a third curve k vs. α intersects with the previous ones at the same point, only if there is damage. A fourth curve k vs. α would continue intersecting with the previous ones in the same point, which is why it is dispensable.

In this approach, an algorithm has been developed to solve the inverse method by means of the software "Mathematica" [23]. The algorithm has been performed to obtain, for each eigenvalue β, the curves $k(\alpha)$ and also the curves $r(\alpha)$. It is pointed out that the curves $r(\alpha)$ allow a direct reading of both position and depth of the crack, which is a novel contribution for obtaining the results.
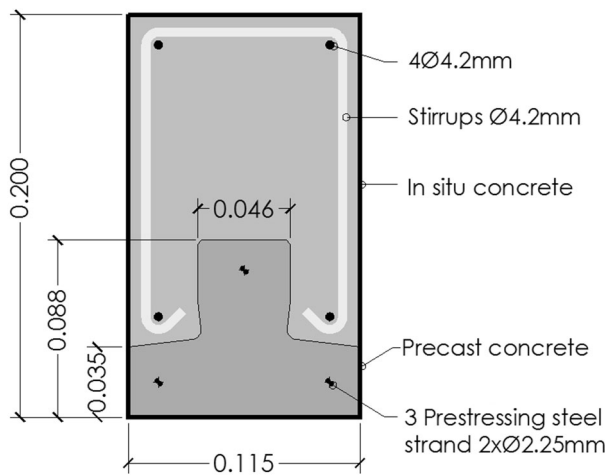
(dimensions in meters)

Fig. 6 Cross section of the beams tested in the laboratory

3 Experimental methodology

Laboratory tests were performed for two similar beams, with different positions of the damage. Beam 01 was cracked in its central area and Beam 02 in a position near one of its ends.

3.1 Characteristics of beams

The beams were built with a precast beam of prestressed concrete to which a compression head of in situ concrete was added. In Fig. 6, the cross section of the beams is shown. To achieve a good adhesion between the in situ concrete and the precast beam, an epoxy adhesive has been used. The total length of the beams was 2.20 m. Precast concrete and in situ concrete were class C30/37 according to the specifications of the precast beams' manufacturer and compression tests of the in situ concrete. The tensile strength of prestressing steel was 1950 MPa.
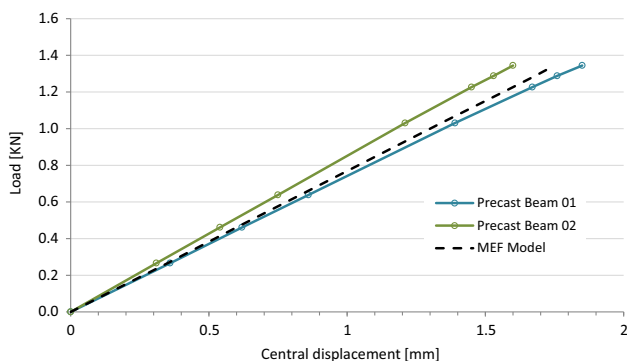
To verify the mechanical behavior of the precast beams, a bending test was carried out. The simply supported precast beams were subject to controlled loads and the vertical displacements in the center of the span were measured. The distance between the supports was 2.00 m and the load was applied in the central area of the span, equally distributed in two points separated from each other by 0.50 m. This test allowed to adjust the properties of the material in a model performed with the finite element method, by imposing in the model the displacements measured in the test. As result, an approximation for the elastic modulus of the concrete of $E_H = 30$ GPa was achieved. The results of the bending tests compared to the FEM can be seen in Fig. 7.

3.2 Description of tests

The simply supported beams, 2.00 m span, were subjected to a point load. The point load in Beam 01 was applied in the midspan, while the point load in Beam 02 was applied closer to one of its ends. In both cases, the point load was increased until a discrete crack in the beam was caused. At this time, the depth of the crack and its position were measured. Then, the point load was suppressed and the crack was closed due to the prestressing action.

Figure 8 shows Beam 01 while the point load is applied. In this figure, the loading press, the load cell and the fleximeters installed on the beam that provide data regarding the vertical displacements can be seen. In Fig. 9, a load–displacement diagram obtained for this beam can be seen. Figure 10 shows the crack caused to Beam 01, for the maximum load applied of 19.06 KN and Fig. 11 shows the depth and maximum width of the crack. These values were: 0.062 m for the crack depth ($r = 0.31$) and 0.35 mm for its maximum width. The position of the crack was $\alpha = 0.485$. Figure 12 shows the zone of the crack once Beam 01 was unloaded; the crack is not visible because the prestressing closes it.

On the other hand, for Beam 02, the crack depth was $r = 0.535$ (Fig. 13) and the position $\alpha = 0.80$. Table 1 summarizes the position and magnitude of the cracks for both beams.
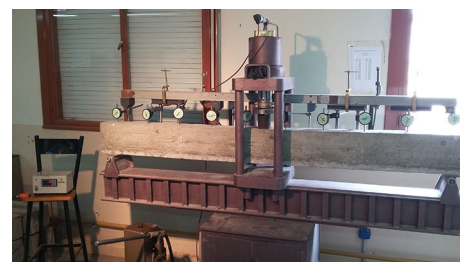

Fig. 7 Load vs. central displacement for the precast beams

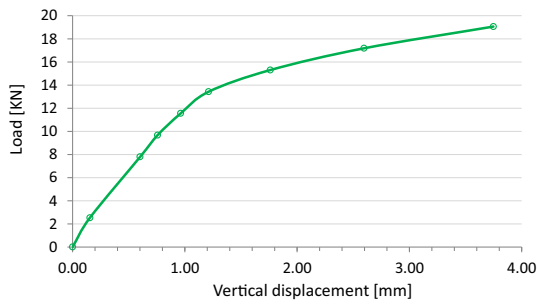**Fig. 8** View of Beam 01 when the crack was caused

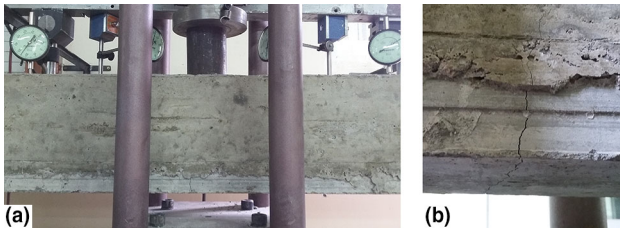**Fig. 9** Load vs. displacement in the point $x/L = 0.44$ for Beam 01

Fig. 10 Crack of Beam 01. **a** General view. **b** Detailed view
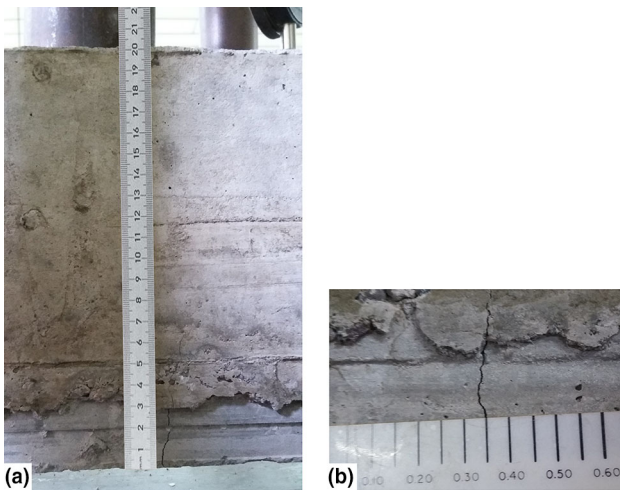

Fig. 11 Measurement of the crack in Beam 01. **a** Depth. **b** Maximum width

Fig. 12 Zone of the crack in Beam 01 after unloading. The crack is closed and not visible

Fig. 13 Crack of Beam 02

Table 1 Position and depth of the crack for both beams

	Position (α)	Depth (r)
Beam 01	0.485	0.310
Beam 02	0.800	0.535

Next, the first three natural frequencies of the damaged beams were obtained. It is noteworthy that previously, this was also performed for the beams without damage for comparative purposes. To obtain the natural frequencies, an accelerometer (5 g) connected to a data acquisition system [24] was used. The accelerometer was placed in a quarter of the beam span. Then a dynamic excitation by a stroke in the opposite quarter of the beam span was caused. In this way, the excitation and measurement of the first three natural frequencies are achieved, since the positions
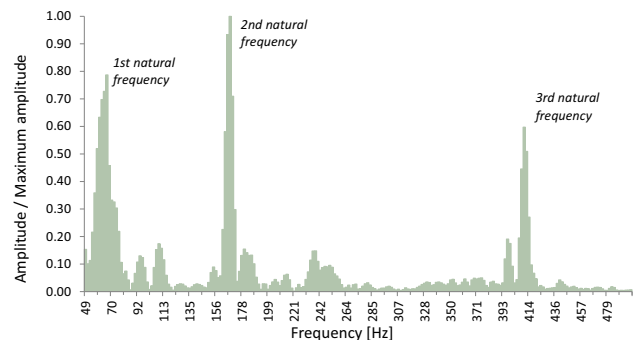

Fig. 14 Frequency spectrum of Beam 01 without damage

Fig. 15 Frequency spectrum of the cracked Beam 01

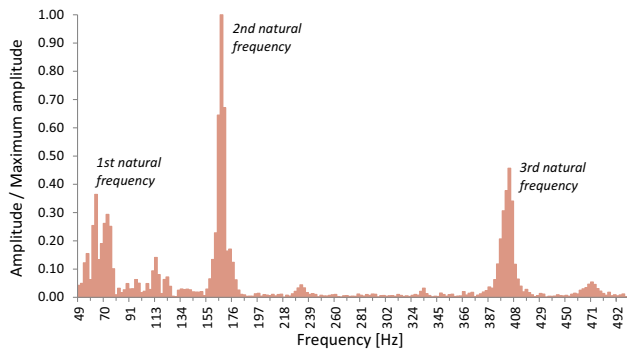**Fig. 16** Frequency spectrum of Beam 02 without damage

Fig. 17 Frequency spectrum of the cracked Beam 02

of the hit and the accelerometer do not coincide with the nodes of the vibration modes. For comparative purposes, the frequency measurements were repeated and the same results were verified. The possibility of using a single accelerometer demonstrates the easy application of this method of damage detection.

After measuring the acceleration in the time domain, this signal was processed by the software "*Logger Pro*" [25], in which the amplitudes in the frequency domain were obtained through Fourier transform. Thus, the first three natural frequencies of vibration were observed. The frequency spectrums are shown in Figs. 14 and 15 for Beam 01 without damage and that with crack, respectively. It is highlighted that to obtain frequencies up to 500 Hz, it was necessary to use a data acquisition speed of 1000 samples/s, according to the Nyquist [26]–Shannon [27] sampling theorem. The values of the natural frequencies obtained for Beam 01 are shown in Table 2. It can be noted that the second natural frequency was the least changed by the cracking because the crack is close to a node of this mode shape.

On the other hand, Figs. 16 and 17 show the frequency spectrums for Beam 02, while Table 3 shows the values of its first three natural frequencies. In this case, it can be noted that the second natural frequency was the most changed by the cracking, because the crack is close to an anti-node of this mode shape.

Table 3 Natural frequencies of Beam 02 in both conditions: without damage and cracked

Modal shape	1	2	3
B02 without damage	72.3 Hz	169.9 Hz	406.2 Hz
B02 cracked	66.4 Hz	148.4 Hz	367.2 Hz
Variation	− 8.2%	− 12.7%	− 9.6%

4 Application of the inverse method

From the first three natural frequencies of the damaged beams, the IM was applied through the algorithm developed by the authors. Since the algorithm has been developed for a theoretical model, it is necessary to consider a correction factor over the frequencies measured in the experimental models. For this reason, first, the frequencies of the theoretical model of the beam without damage were compared with the frequencies of a model made with the finite element method (FEM). Then, a correction factor χ_1, which takes into account the real site of the end supports, was calculated. In other words, the theoretical model considers the supports placed on the neutral axis, while in the laboratory model the supports were placed on the lower surface of the beam. Another difference that includes this

Table 2 Natural frequencies of Beam 01 in both conditions: without damage and cracked

Modal shape	1	2	3
B01 without damage	66.4 Hz	167.0 Hz	411.1 Hz
B01 cracked	63.3 Hz	166.4 Hz	402.1 Hz
Variation	− 4.7%	− 0.4%	− 2.2%

correction factor is that in the theoretical model the beam ends exactly on the supports, while in the laboratory model the beams end 0.10 m beyond each support.

Also for the beam without damage, the frequencies measured in the laboratory were compared with those obtained by the FEM. In this case, a second correction factor χ^2 was calculated This factor considers the differences between experimental measurements and results obtained for the numerical models, which may be due to variations in concrete properties, possible geometric imperfections, etc. In addition, this factor takes into account the structural damping, which is always present in the real model and has not been considered in the numerical models; however, for structural low damping ratios ($< 20\%$, according to Clough and Penzien [28]) there is no significant difference between the undamped and damped natural frequencies.

The FEM model was obtained with the software "*Comsol Multiphysics*" [29]. It has been used as a 3D model with a mesh of tetrahedral elements for both materials: concrete and steel [30, 31]. The prestressing forces were introduced by an initial deformation of steel. The materials of the model were considered to be homogeneous, continuous and isotropic with linear behavior. The properties of the materials are—elastic modulus of concrete: $E_H = 30$ GPa, Poisson's ratio of concrete: $v_H = 0.20$, elastic modulus of steel: $E_A = 200$GPa and Poisson's ratio of steel: $v_A = 0.30$. These properties, adopted in the numerical models, were verified by comparing the results of experimental bending tests for both precast and composite beams.

Table 4 shows the values of the first three natural frequencies for Beam 01 without damage. The frequencies of the different models can be seen: theoretical, numerical and experimental. This table also includes the two corresponding correction factors. The values of theoretical frequencies were obtained from the following equation:

$$f_i[Hz] = \beta_i^2 \frac{c}{2\pi}, \tag{13}$$

where i corresponds to the i vibration mode, and for a simply supported beam:

Table 4 Natural frequencies of Beam 01 without damage and the correction factors

Modal shape	1	2	3
Theoretical frequencies	80.401 Hz	321.602 Hz	723.605 Hz
FEM frequencies	73.925 Hz	242.288 Hz	622.346 Hz
Experimental frequencies	66.4 Hz	167.0 Hz	411.1 Hz
Correction factors χ^1	1.088	1.327	1.163
Correction factors χ^2	1.113	1.451	1.514

$$\beta_i = i\pi, \tag{14}$$

while c, defined in Eq. (4), in this case is calculated for the homogenized cross section from the following values: $E = 30.0$ GPa, $I = 7.7731 \times 10^{-5}$ m^4, $\rho = 2385.52$ kg/m^3, $A = 0.023194$ m^2, $L = 2.00$ m.

Although in some cases the correction factors are very distant from 1, it should be considered that when a real structure of a certain age is inspected, its behavior will probably also be very different from the theoretical model.

Finally, the first three natural frequencies measured in the laboratory for the cracked beam were corrected with Eq. (15) and introduced into the algorithm developed for the application of the inverse method.

$$f c_{cb} = f e_{cb} \chi_1 \cdot \chi_2, \tag{15}$$

where $f c_{cb}$ is the corrected frequency of the cracked beam and $f e_{cb}$ is the experimental frequency of the cracked beam.

Table 5 shows the corrected natural frequencies of the cracked Beam 01. These values have been introduced into the IM algorithm, and the curves $k(\alpha)$ shown in Fig. 18 have been obtained. In Fig. 18, the curves $k(\alpha)$ intersect each other at two points because of the symmetry, with one of them being the position of the crack. It is important to mention that the intersection is not exactly at one point, but occurs in a triangular approach zone.

Moreover, for a beam of rectangular cross section, the spring stiffness can be related to the depth of the crack through Eq. (9) [12, 13] and the curves $r(\alpha)$ can be directly obtained. However, this equation is applicable to homogeneous materials and does not consider the effect of prestressing, which tries to keep the crack closed. Therefore, in this case, it is expected that the results underestimate the magnitude of the real crack. In Fig. 19, plots $r(\alpha)$ are shown for Beam 01. Since the intersection of the three curves is not exactly a point, a zoom of the intersection zone is represented in Fig. 20, in which the barycenter is found and is considered to be the point of intersection. Figure 20 shows the inverse method of detecting the crack at the position $\alpha = 0.438$, with a depth parameter $r = 0.205$. The absolute error in the detection of the damage position, given by the difference between the real position of the crack ($\alpha = 0.485$) and the position obtained with the IM, resulted in -4.7%. On the other hand, because the real depth of the crack is $r = 0.31$, the IM gives an absolute error of -10.5% in its prediction.

To compare the results for both conditions, damaged and non-damaged beam, the curves $k(\alpha)$ for the beam without damage have been plotted in Fig. 21. In this figure, it can be noted that there is no intersection point of the three curves. In addition, these curves reach rigidity values much higher than in the case of the damaged beams.

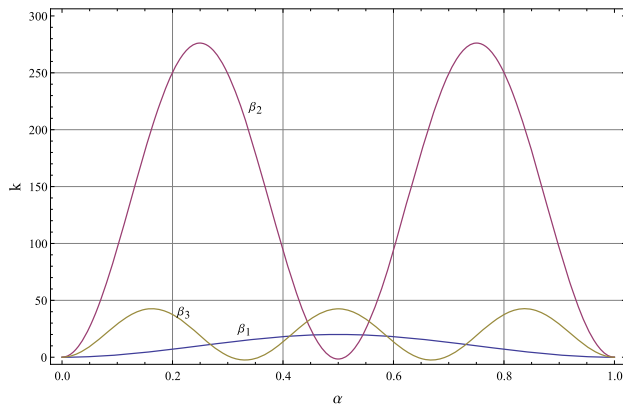| Table 5 Corrected natural frequencies of the cracked Beam 01	Modal shape	1	2	3
	Corrected frequencies of cracked B01	76.647 Hz	320.447 Hz	707.764 Hz

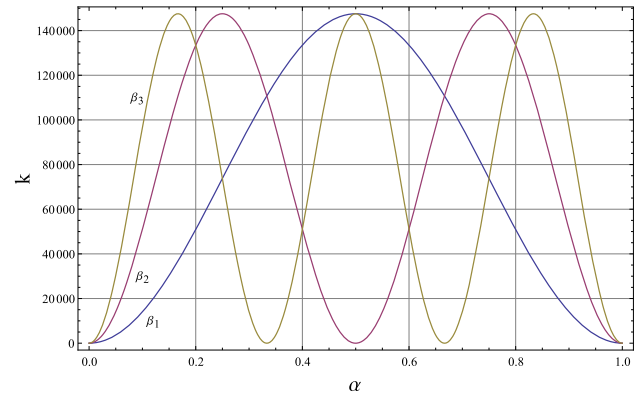Fig. 18 Plots of k vs. α for the first three natural frequencies of the cracked Beam 01
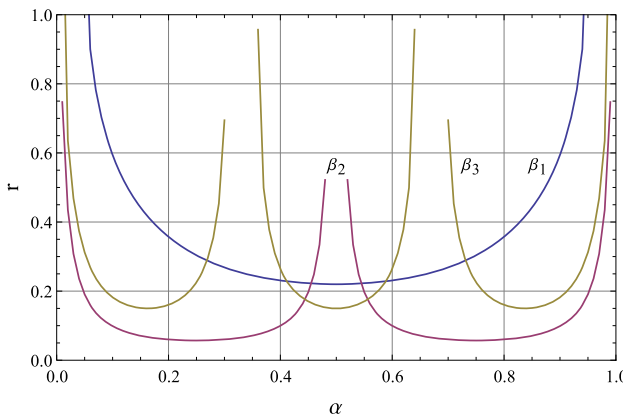

Fig. 19 Plots of r vs. α for the first three natural frequencies of the cracked Beam 01
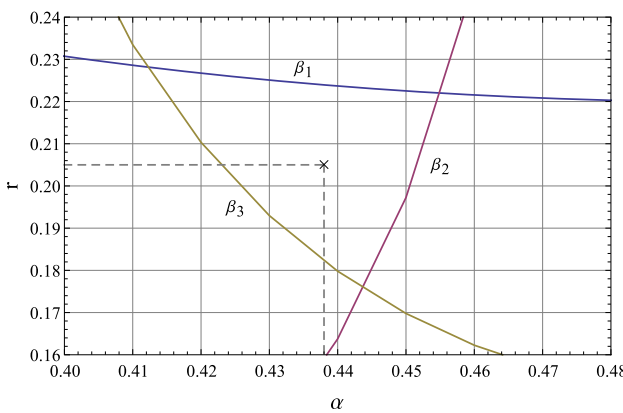

Fig. 20 Idem Fig. 19; zoom in the intersection zone of the three curves

Fig. 21 Plots of k vs. α for the first three natural frequencies of the beam without damage

Table 6 Natural frequencies of Beam 02 without damage and the correction factors

Modal shape	1	2	3
Theoretical frequencies	80.401 Hz	321.602 Hz	723.605 Hz
FEM frequencies	73.925 Hz	242.288 Hz	622.346 Hz
Experimental frequencies	72.3 Hz	169.9 Hz	406.2 Hz
Correction factors χ^1	1.088	1.327	1.163
Correction factors χ^2	1.022	1.426	1.532

Similar to Beam 01, the inverse method was applied to Beam 02. Table 6 shows the first three natural frequencies of vibration for Beam 02 without damage, using the three different models previously mentioned: theoretical, FEM and experimental. This table also includes the two corresponding correction factors. Then, Table 7 shows the first three natural frequencies of the cracked Beam 02 modified by the correction factors. These values have been introduced into the IM algorithm and the results have been represented in Figs. 22, 23 and 24.

Figure 24 shows the detection of the crack at the position $\alpha = 0.780$, with a depth parameter $r = 0.410$. The absolute error in the detection of the damage position, given by the difference between the real position of the crack ($\alpha = 0.800$) and the position obtained with the IM was − 2.0%. In the prediction of the crack depth, the IM gave an absolute error of − 12.5%, since the real depth of the crack was $r = 0.535$.

Table 7 Corrected natural frequencies of the cracked Beam 02

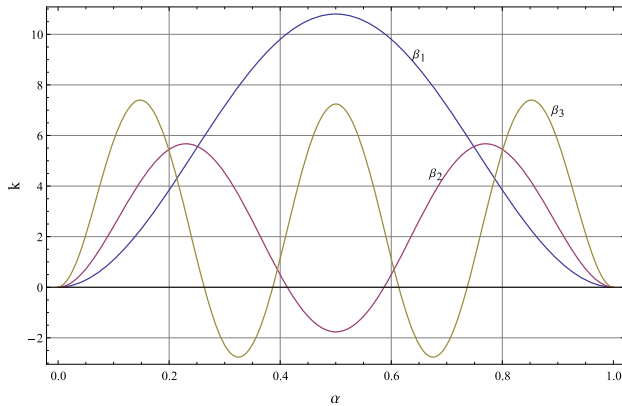| Modal shape	1	2	3
Corrected frequencies of cracked B02	73.840 Hz	280.905 Hz	654.131 Hz

Fig. 22 Plots of k vs. α for the first three natural frequencies of the cracked Beam 02
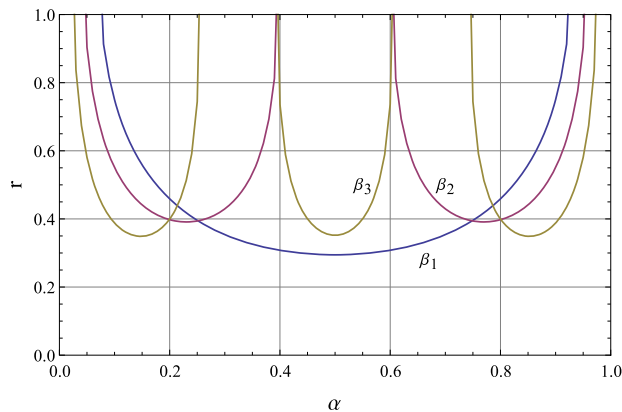

Fig. 23 Plots of r vs. α for the first three natural frequencies of the cracked Beam 02
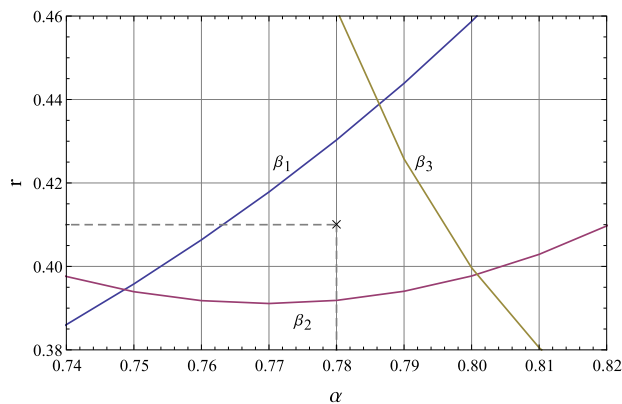

Fig. 24 Idem Fig. 23; zoom in the intersection zone of the three curves

5 Conclusions

In this work, the inverse method has been applied to detect damage in two prestressed concrete beams built in the laboratory. This method is based on the analysis of the dynamic behavior of the structure and allows to obtain the position and depth of a discrete crack present in the beam. To solve the system of equations, an algorithm has been developed. From the experimental results, the following conclusions are highlighted:

– The application of the IM allowed the detection of damage for two different experimental models: one of the models with the crack in the central area and the other with the crack near one of the end supports.
– Although the IM gives two possible locations of damage, because of the symmetry of the beam only one of them corresponds to the real crack position.
– The absolute errors for the prediction of the crack position, obtained with the IM, are -4.7 and -2.0% for Beam 01 and Beam 02, respectively. The authors consider these errors acceptable for an experimental work.
– For the crack depth, the absolute errors obtained by the IM algorithm are -10.5 and -12.5%, for Beam 01 and Beam 02, respectively. It is important to note that both the uncertainties in the concrete properties and the effects of the prestressing force have not been taken into account in the present work. Therefore, future studies that consider the influence of the prestressing force to determine the crack depth may also be necessary.
– The application of the IM has been of simple practical implementation.
– Despite that the inverse method is well known for its application to materials such as reinforced concrete and steel, this work presents a way to apply the same method considering the health monitoring of pre-stressed concrete beams.

References

1. Karayannis CG, Chalioris CE (2013) Design of partially pre-stressed concrete beams based on the cracking control provisions. Eng Struct 48:402–416. https://doi.org/10.1016/j.engstruct.2012.09.020

2. Yao Y, Tung S-TE, Glisic B (2014) Crack detection and characterization techniques—an overview. Struct Control Health Monit 21:1387–1413. https://doi.org/10.1002/stc.1655

3. Dai L, Wang L, Zhang J, Zhang X (2016) A global model for corrosion-induced cracking in prestressed concrete structures. Eng Fail Anal 62:263–275. https://doi.org/10.1016/j.engfailanal.2016.01.013

4. Darmawan SM, Stewart MG (2007) Spatial time-dependent reliability analysis of corroding pretensioned prestressed concrete bridge girders. Struct Saf 29:16–31. https://doi.org/10.1016/j.strusafe.2005.11.002

5. Lee BY, Koh KT, Ismail MA, Ryu HS, Kwon SJ (2017) Corrosion and strength behaviors in prestressed tendon under various tensile stress and impressed current conditions. Adv Mater Sci Eng. https://doi.org/10.1155/2017/8575816

6. Calavera J (2005) Patología de Estructuras de Hormigón Armado y Pretensado, 2nd edn. Intemac Ediciones, Madrid

7. CEB-FIP (1993) Model code 1990: Design code. T. Telford, London

8. Comisión Permanente del Hormigón (2011) EHE-08 Instrucción de Hormigón Estructural (5th ed.) Ministerio de Fomento, Madrid

9. Centro de Investigación de los Reglamentos Nacionales de Seguridad para las Obras Civiles (2005) CIRSOC 201 Reglamento Argentino de Estructuras de Hormigón. INTI, Buenos Aires

10. American Concrete Institute (2014) ACI 318-14: building code requirements for structural concrete and commentary. American Concrete Institute, Farmington Hills

11. Unger JF, Teughels A, De Roeck G (2006) System identification and damage detection of a prestressed concrete beam. J Struct Eng 132(11):1691–1698. https://doi.org/10.1061/(ASCE)0733-9445(2006)132:11(1691)

12. Anifantis N, Dimarogonas A (1983) Stability of columns with a single crack subjected to follower and vertical loads. J Solids Struct 19(4):281–291. https://doi.org/10.1016/0020-7683(83)90027-6

13. Ostachowicz WM, Krawczuk M (1991) Analysis of the effect of cracks on the natural frequencies of a cantilever beam. J Sound Vib 150:191–201. https://doi.org/10.1016/0022-460X(91)90615-Q

14. Rizos PF, Aspragathos N, Dimarogonas AD (1990) Identification of crack location and magnitude in a cantilever beam from the vibration modes. J. Sound Vibration 138(3):381–388. https://doi.org/10.1016/0022-460X(90)90593-O

15. Liang RY, Choy FK, Hu J (1991) Detection of cracks in beam structures using measurements of natural frequencies. J Franklin Inst 328:505–518. https://doi.org/10.1016/0016-0032(91)90023-V

16. Nandwana BP, Maiti SK (1997) Modelling of vibration of beam in presence of inclined edge or internal crack for its possible detection based on frequency measurements. Eng Fract Mech 58:193–205. https://doi.org/10.1016/S0013-7944(97)00078-7

17. Rosales MB, Filipich CP, Buezas FS (2009) Crack detection in beam-like structures. Eng Struct 31:2257–2264. https://doi.org/10.1016/j.engstruct.2009.04.007

18. Orbanich CJ, Rosales MB, Ortega NF, Filipich CP (2009) Detección de fallas en vigas de fundación elástica mediante el método inverso. Mecánica Computacional XXVIII:613–631

19. Mazanoglu K, Sabuncu M (2012) A frequency based algorithm for identification of single and double cracked beams via a statistical approach used in experiment. Mech Syst Signal Process 30:168–185. https://doi.org/10.1016/j.ymssp.2012.02.004

20. Barad KH, Sharma DS, Vyas V (2013) Crack detection in cantilever beam by frequency based method. Procedia Eng 51:770–775. https://doi.org/10.1016/j.proeng.2013.01.110

21. Rao SS (2007) Vibration of continuous systems. Wiley, Hoboken

22. Blevins RD (2001) Formulas for natural frequency and mode shape. Krieger Publishing Company, UK

23. Wolfram S (2015) An elementary introduction to the wolfram language. Wolfram Media, Inc

24. Vernier (2008) Labquest interfase. Software and Technology, Beaverton, OR, USA

25. Vernier (2008) Logger pro 3.6.1. Software and Technology, Beaverton, OR, USA

26. Nyquist H (1928) Certain topics in telegraph transmission theory. Trans AIEE 47:617–644. https://doi.org/10.1109/T-AIEE.1928.5055024

27. Shannon E (1949) Communication in the presence of noise. Proc Inst Radio Eng 37:10–21. https://doi.org/10.1109/JRPROC.1949.232969

28. Clough RW, Penzien J (1995) Dynamics of structures, 2nd edn. McGrawHill, New York

29. COMSOL (2013) COMSOL Multiphysics User's Guide, Version 4.4

30. Jason L, Ghavamianc S, Courtois A (2010) Truss vs solid modeling of tendons in prestressed concrete structures: consequences on mechanical capacity of a representative structural volume. Eng Struct 32:1779–1790. https://doi.org/10.1016/j.engstruct.2010.02.029

31. Yapar O, Basu PK, Nordendale N (2015) Accurate finite element modeling of pretensioned prestressed concrete beams. Eng Struct 101:163–178. https://doi.org/10.1016/j.engstruct.2015.07.018